FREE-FLIGHT INVESTIGATIONS OF SUBLIMING ABLATORS AND TRANSPIRATION COOLING AT HYPERSONIC VELOCITIES

By Thomas E. Walton, Jr., Bernard Rashis,
and Clyde W. Winters

NASA Langley Research Center
Langley Station, Hampton, Va.

Presented at the AIAA-ASD Vehicle Design and Propulsion Meeting

Dayton, Ohio
November 4-6, 1963

FREE-FLIGHT INVESTIGATIONS OF SUBLIMING ABLATORS AND TRANSPIRATION COOLING AT HYPERSONIC VELOCITIES

Thomas E. Walton, Jr., Bernard Rashis, and Clyde W. Winters
Aerospace Engineers, Applied Materials and Physics Division
NASA Langley Research Center

15524

Summary

The results of several free-flight investigations, in which the thermal protection was provided by either a subliming ablator or by transpiration cooling, are discussed. The flight-test regime covered an altitude band from about 177,000 feet to 25,000 feet and peak velocities ranged from 3,900 feet per second to 22,200 feet per second.

The similarities between subliming ablators and transpiration cooling are described and it is shown how the effectiveness of ablation materials can be predicted accurately from transpiration data. This analytical procedure permits direct comparison of the two types of heat protection and allows extrapolation, based on low-speed transpiration data, of ablation material effectiveness to supercircular velocities.

Introduction

Mass injection, either by ablation or transpiration, can reduce the net heat transfer from the hot-gas stream in the boundary layer to the surface by an appreciable amount. In addition, mass injection at a leading edge or stagnation point offers protection to surfaces downstream by the film-cooling process. In the past, numerous ground tests have been conducted employing these cooling systems. Since the simulation of actual flight conditions in ground facilities is seldom achieved (e.g., duplicating the conditions a spacecraft would encounter upon reentering the earth's atmosphere at supercircular velocities), the Langley Research Center initiated a flight-test research program that would provide information in an actual flight environment.

The investigations were conducted employing solid-fuel rocket-propelled vehicle systems. The number of rocket stages used varied from three to five depending on the performance required for each individual experiment. One of the vehicle systems utilized the NASA developed Scout booster.

The results of several free-flight investigations, covering an altitude range from 177,000 feet to 25,000 feet and peak velocities of 3,900 feet per second to 22,200 feet per second, are discussed. Thermal protection in these experiments was provided by either subliming ablators or by transpiration cooling. Furthermore, it is shown how the material effectiveness of subliming ablators may be determined, simply and directly, from transpiration cooling results. This permits direct comparison between the two types of heat protection and, more significantly allows extrapolation, based on low-speed transpiration data, of ablation material effectiveness to supercircular velocities.

Symbols

c_p specific heat, Btu/lb-$^{\circ}$F

F ratio of coolant mass-flow rate to local air mass-flow rate

f fraction of vaporization

H enthalpy, Btu/lb

h_{eff} effective heat of ablation

h_{ov} material intrinsic heat capacity, Btu/lb

$\dot{m}$ ablation rate, lb/(sq ft)(sec)

n temperature ratio exponent

N_{St} Stanton number

q heat-transfer rate, Btu/(sq ft)(sec)

T temperature, $^{\circ}$F

Subscripts:

aw adiabatic wall

c coolant

ℓ local (just outside of the boundary layer)

0 zero injection or uncooled case

w wall

w,air air at wall temperature

Models and Instrumentation

A typical model design used to investigate both transpiration and downstream cooling is shown in figure 1. The particular configuration shown is a solid conical body having a blunt nose cap made of porous stainless steel. Nitrogen gas is released from the accumulator at a predetermined time during the flight test. The nitrogen coolant flow rate is determined from measurements of the pressure differential across the porous nose and the pressure and temperature of the gas in the nose chamber. Thermocouples are spotwelded to the back side of the porous nose cap and of the conical afterbody to measure the heat transfer with coolant injection through the porous nose.

A typical Teflon ablation model, instrumented with variable-capacitance ablation rate sensors, is shown in figure 2. The variable-capacitance ablation rate sensor which continuously measures the ablation rate of Teflon was developed by NASA. Details of the design, construction, and calibration technique are given in reference 1; the sensor is shown schematically in figure 3.

Test Regime

Figure 4 is a plot of the test regime for the flight investigations. The altitude band covered by the different flight tests ranged from about 25,000 feet to 177,000 feet and the peak velocities ranged from 3,900 ft/sec to 22,200 ft/sec. The corresponding enthalpy range was approximately 190 Btu/lb to 10,000 Btu/lb. The dynamic pressure varied from 100 lb/ft^2 to 7,000 lb/ft^2 and the free-stream Reynolds number per foot varied from 0.5×10^6 to 6×10^6.

In addition to the flight tests a number of ground tests were conducted in a Mach number 2.0 ethylene heated high-temperature air jet. The Reynolds number range based on 1 foot varied from about 12×10^6 at a stagnation enthalpy of 250 Btu/lb to 2×10^6 at a stagnation enthalpy of 800 Btu/lb. The dynamic pressure was approximately 5,200 lb/ft^2.

Transpiration Cooling Results and Analysis

The results of two flight tests and a number of ground tests[2,3] utilizing the technique of transpiration cooling, are summarized in figure 5 where the shielding effect ratio $\frac{N_{St}}{N_{St,0}}$ is expressed as a function of the nondimensional flow-rate parameter $\frac{F}{N_{St,0}} \frac{c_{p,c}}{c_{p,l}} \left(\frac{T_l}{T_w}\right)^n$. The lower curve of figure 5 shows the experimental free-flight results to a maximum velocity of 10,400 ft/sec taken from reference 2 where large rates of nitrogen were used for the coolant. Also shown are the theoretical results for relatively moderate rates of mass injection from reference 4 for a three-dimensional laminar stagnation boundary layer. The theoretical results of reference 4 were for several values of T_l/T_w ranging from 1/2 to 4; the authors of reference 5, however, correlated the results by including the temperature ratio in the nondimensional flow-rate parameter with n equal to 0.19. The flight data of reference 2, with large rates of mass injection, correlate well with theory for relatively moderate rates of mass injection also by including the temperature ratio in the nondimensional flow-rate parameter. The ratio $\left(\frac{T_l}{T_w}\right)^{0.19}$ for the experimental flight data of reference 2 extended over a range from 1.45 to 1.66. Examination of the experimental flight data shows a significant heat-transfer reduction due to transpiration cooling. The experimental results shown in figure 5 provide an extension of existing theory to large rates of mass injection.

The upper curve of figure 5 represents the theoretical results for a turbulent boundary layer computed from the relation (obtained from ref. 6 for $T_l/T_w = 1$)

$$\frac{N_{St}}{N_{St,0}} = \frac{\frac{F}{N_{St,0}} \frac{c_{p,c}}{c_{p,l}}}{\exp\left(\frac{F}{N_{St,0}} \frac{c_{p,c}}{c_{p,l}}\right) - 1}$$

Also shown are the experimental results from reference 3 in free flight to a maximum velocity of 3,910 ft/sec and also in a Mach 2.0 ground test facility. The turbulent results from both the ground and flight tests were correlated in a similar manner, as cited previously, for the laminar results by including the temperature ratio in the nondimensional flow-rate parameter. The value of n for the turbulent results was found to be equal to 1.3.

Figure 6 shows the variation of the downstream cooling temperature parameter $\frac{T_w - T_c}{T_{aw} - T_c}$ as a function of the flow-rate parameter $\frac{F}{N_{St,0}} \frac{c_{p,c}}{c_{p,l}}$ for two tests. The center curve of figure 6 shows the free-flight test results to a maximum velocity of 6,020 ft/sec from reference 2, for a laminar boundary layer with a zero pressure gradient. The upper curve, included for comparison, represents the data of reference 7 for a turbulent zero-pressure-gradient boundary layer in a Mach 2.0 ground test facility. Comparison of the results for the two types of boundary layers indicates that, for the same coolant flow rate, lower surface temperatures are achieved in a laminar boundary layer with downstream cooling.

The lower curve shown in figure 6 represents the theoretical results for a porous wall in a turbulent boundary layer.[6] Examination of the curves shows that for the same flow rate of coolant, lower wall temperatures will result on the completely porous wall. Under certain conditions, however, it is possible to maintain solid surfaces at a safe temperature level and use less coolant with a downstream cooling system, since the maximum allowable temperatures of porous materials are generally a great deal lower than for solid materials.

Ablation Results and Analysis

The effectiveness of subliming ablation materials can be derived simply and directly from transpiration cooling results, since the cooling mechanism of this category of ablation materials is analogous to transpiration cooling. Once the relationship between $\frac{N_{St}}{N_{St,0}}$ and $\frac{F}{N_{St,0}} \frac{c_{p,c}}{c_{p,l}} \left(\frac{T_l}{T_w}\right)^n$ is known from transpiration data the effective heat of ablation h_{eff} can be determined. The transformation relationships are:

$$\frac{h_{eff}}{h_{ov}} = \frac{N_{St,0}}{N_{St}} \tag{1}$$

$$\frac{f\left(H_{aw} - H_{w,air}\right)}{h_{ov}} \left(\frac{c_{p,c}}{c_{p,l}}\right) \left(\frac{T_l}{T_w}\right)^n = \frac{\frac{F}{N_{St,0}} \frac{c_{p,c}}{c_{p,l}} \left(\frac{T_l}{T_w}\right)^n}{\frac{N_{St}}{N_{St,0}}} \tag{2}$$

where the terms on the right-hand side of the equation are the pertinent transpiration parameters. Hence, the transformation relationships enable the solution of h_{eff} in terms of the enthalpy difference across the boundary layer $\left(H_{aw} - H_{w,air}\right)$ and

h_{ov}, the intrinsic heat capacity of the material, which is defined as the absorbing capacity of a material prior to ablation. The factor f is the fraction of melt that vaporizes for a melting-vaporizing ablation material. For the present results, f is equal to 1.0, since this paper deals only with subliming ablators. However, the above relationships should also apply to materials in the melting-vaporizing class upon inclusion of the pertinent material property values. Including the specific heat ratio $\frac{c_{p,c}}{c_{p,l}}$ in equation (2) permits shielding results for any coolant to be used in the transformation. Furthermore, including the temperature ratio T_l/T_w in the above relation permits shielding results with any temperature ratio to be used in the transformation where the exponent n varies according to the boundary-layer type. Figure 7 shows the effective heats of ablation curves obtained from theoretical transpiration data of references 4, 6, and 8 for several boundary-layer types. These curves were first presented in reference 5.

As pointed out above, once the shielding relationship is known from transpiration results, the ablation parameters can be derived by the transformation procedure. Figure 8 shows the curves for the effective heats of ablation as a function of the enthalpy parameter for a three-dimensional laminar stagnation boundary layer and also for a turbulent zero-pressure-gradient boundary layer shown previously in figure 5. Also shown are the results from four ablation flight tests. The vertical dashed lines shown in the figure represent the data from two flight tests in which identical results were obtained. The crosses represent the five-stage Scout data. The slanted lines represent the data of reference 9. The velocity variation covered by the ablation tests was from approximately 5,000 ft/sec to 22,200 ft/sec. The values of h_{eff} for the ablation tests were computed from the relation

$$h_{eff} = \frac{q_0}{\dot{m}}$$

where q_0 is the heat transfer to a nonablating surface having the same temperature as the ablating surface. The value of h_{ov} used in the computations was equal to 900 Btu/lb for Teflon. All of the experimental ablation results were successfully correlated with theory for a three-dimensional laminar stagnation boundary layer; for purposes of clarity, however, some of the ablation test data has been displaced from the theory curve.

Figure 9 shows the effective heat of ablation as a function of the enthalpy parameter obtained from the transformed transpiration data of reference 2. Also shown are the ablation flight tests along with theory for a three-dimensional laminar stagnation boundary layer. Since the value of the enthalpy parameter from transformed transpiration data is proportional to the mass injection rate, large rates of mass injection for a transpiration test would simulate a high flight velocity for an ablation test wherein the mass injection rates are relatively low. Although the transpiration flight test of reference 2 was conducted to a maximum velocity of only 10,400 ft/sec, since large rates of mass injection were used, the transformed results permit an extension of theory to supercircular velocities.

Conclusions

The following conclusions are based on the results of several free-flight investigations wherein the thermal protection was provided by either a subliming ablator or by transpiration cooling:

1. The analogous behavior of subliming ablators to transpiration cooling permits direct comparison of these two types of heat protection.

2. Since the effectiveness of ablating materials is proportional to the mass injection rate and the vehicle velocity, extrapolation of the transpiration cooling effect based on relatively low-speed transpiration data, wherein high mass ejection rates were used, permits the prediction of material effectiveness to supercircular speeds.

References

1. Winters, Clyde W., and Bracalente, Emedio M.: A Sensor for Obtaining Ablation Rates. NASA TN D-800, 1961.

2. Walton, Thomas E., Jr.: Free-Flight Investigation of Mass Transfer Cooling on Both a Porous Nose and a Nonporous Conical Afterbody to a Mach Number of 10.6. (Prospective NASA TN.)

3. Walton, Thomas E., Jr., and Rashis, Bernard: Measurement and Empirical Correlation of Transpiration Cooling Parameters on a 25° Cone in a Turbulent Boundary Layer in Both Free Flight and a Hot-Gas Jet. NASA TN D-967, 1961.

4. Reshotko, Eli, and Cohen, Clarence B.: Heat Transfer at the Forward Stagnation Point of Blunt Bodies. NACA TN 3513, 1955.

5. Rashis, Bernard, and Hopko, Russell N.: An Analytical Investigation of Ablation. NASA TM X-300, 1960.

6. Leadon, B. M., and Scott, C. J.: Measurement of Recovery Factors and Heat Transfer Coefficients with Transpiration Cooling in a Turbulent Boundary Layer at M = 3.0 Using Air and Helium as Coolants. Res. Rep. No. 126 (Contract AF 18(600)-1226), Inst. Tech., Dept. Aero. Eng., Univ. of Minnesota, Feb. 1956.

7. Witte, William G., and Rashis, Bernard: An Experimental Investigation and Correlation of the Heat Reduction to Nonporous Surfaces Behind a Porous Leading Edge Through Which Coolant is Ejected. NASA TM X-235, 1960.

8. Brown, W. Byron, and Donoughe, Patrick L.: Tables of Exact Laminar-Boundary-Layer Solutions When the Wall is Porous and Fluid Properties are Variable. NACA TN 2479, 1951.

9. Winters, Clyde W., Witte, William G., Rashis, Bernard, and Hopko, Russell N.: Free-Flight Investigation of Ablation of a Blunt Body to a Mach Number 13.1. NASA TN D-1500, 1962.

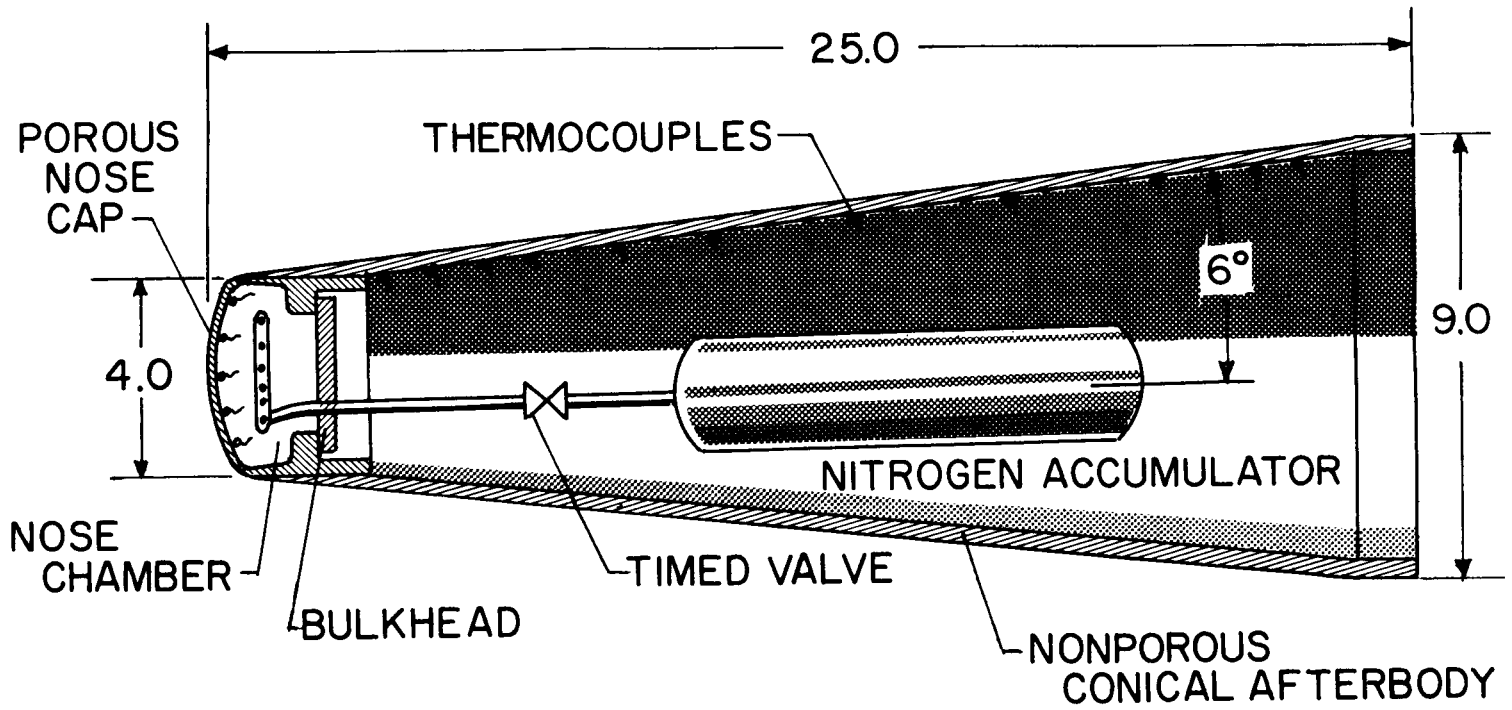

Figure 1.- Transpiration and downstream cooling model.

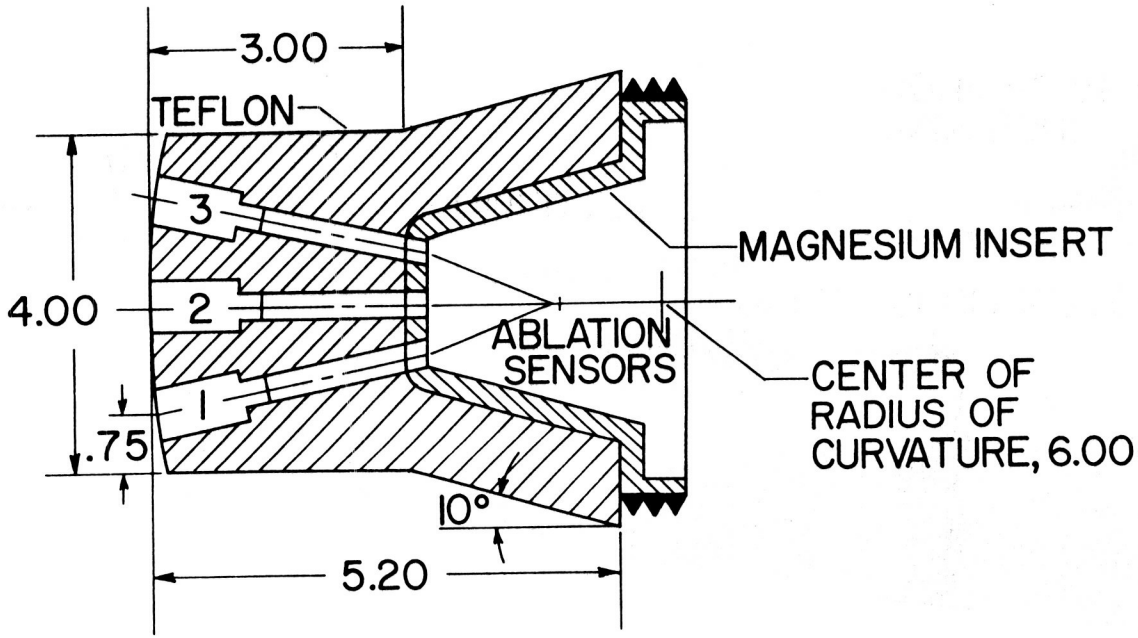

NASA

Figure 2.- Typical ablation model.

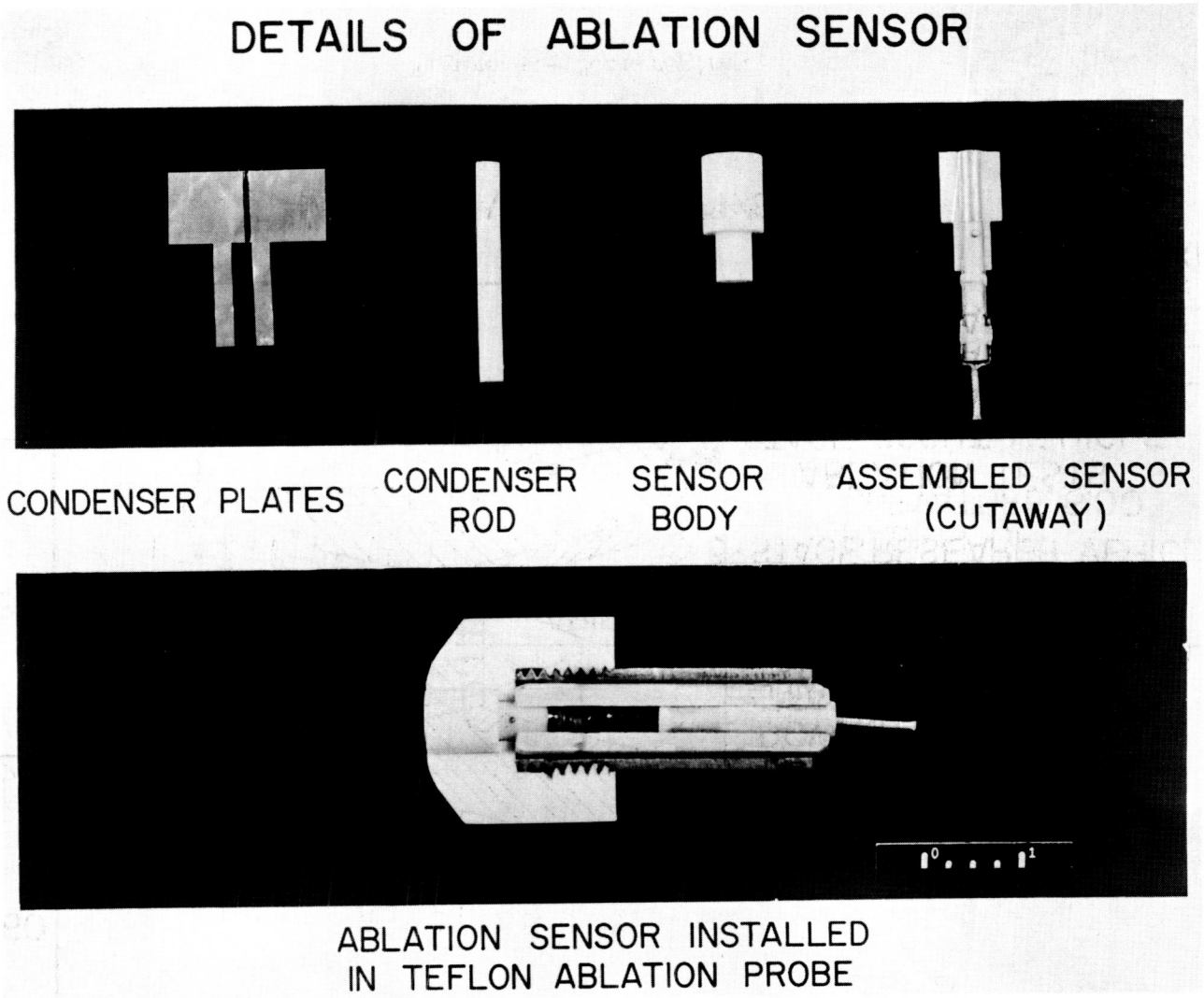

NASA
L-59-4102

Figure 3.- Details of ablation sensor.

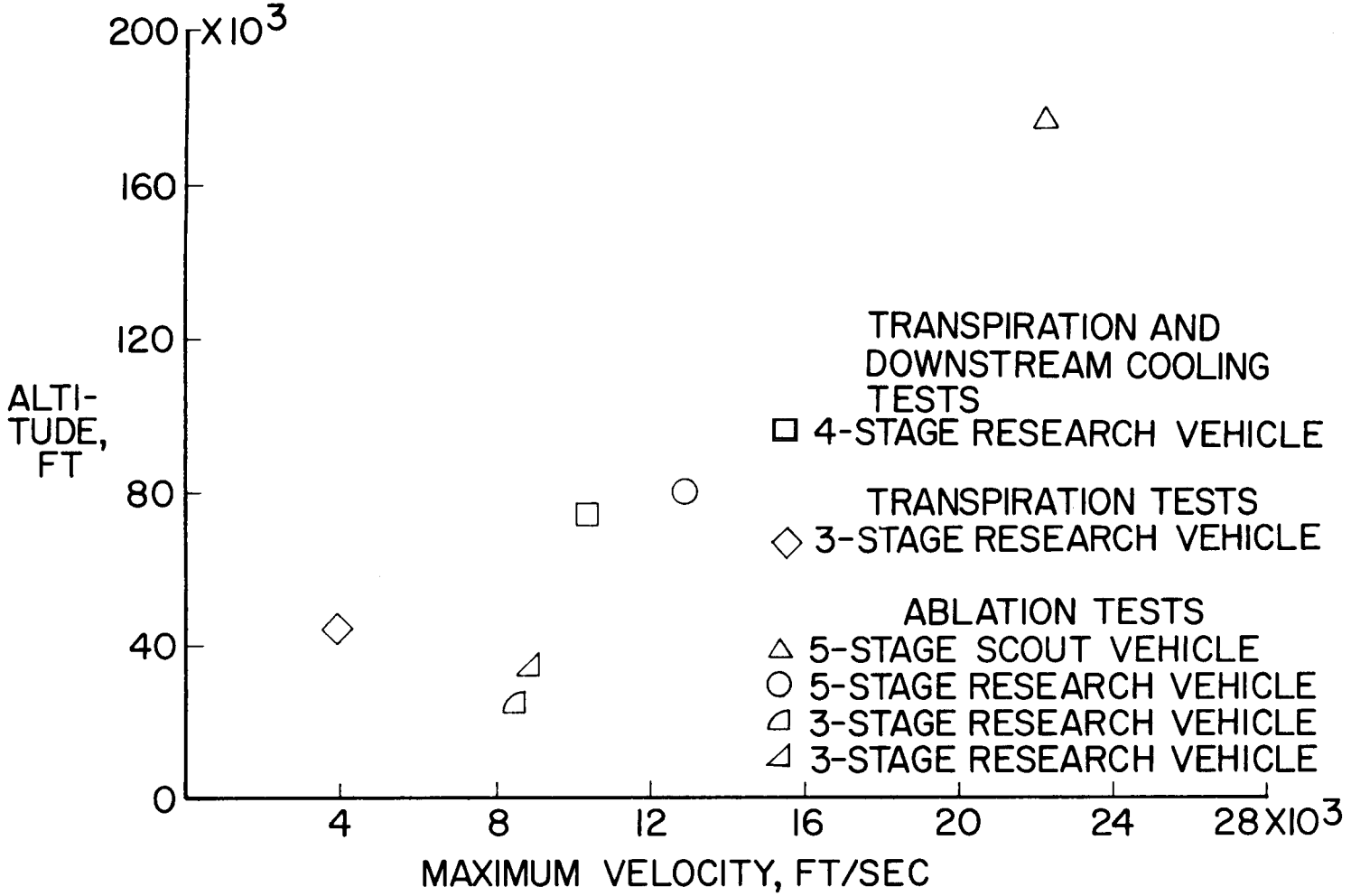

Figure 4.- Test regime.

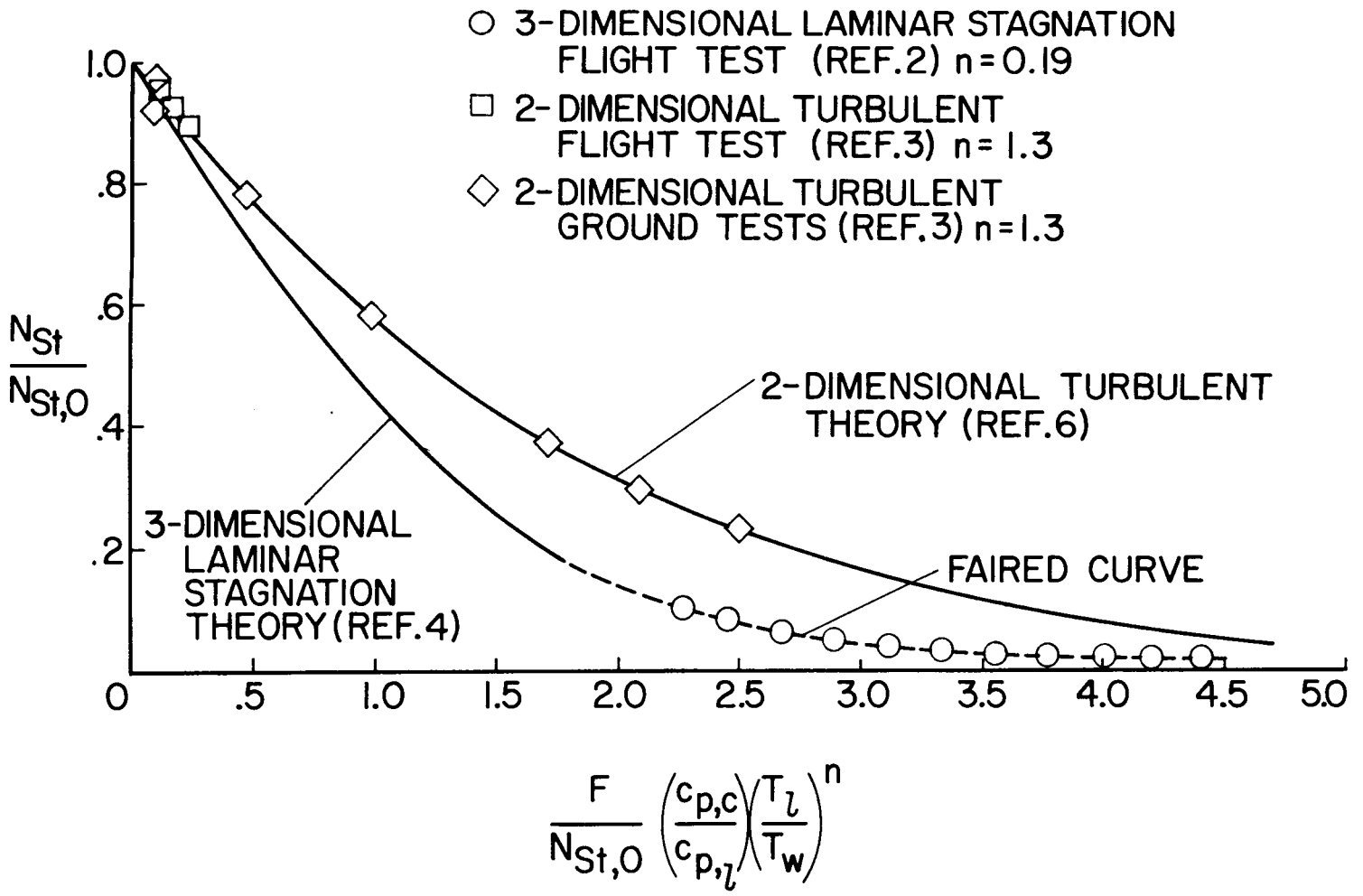

NASA

Figure 5.- Transpiration test results.

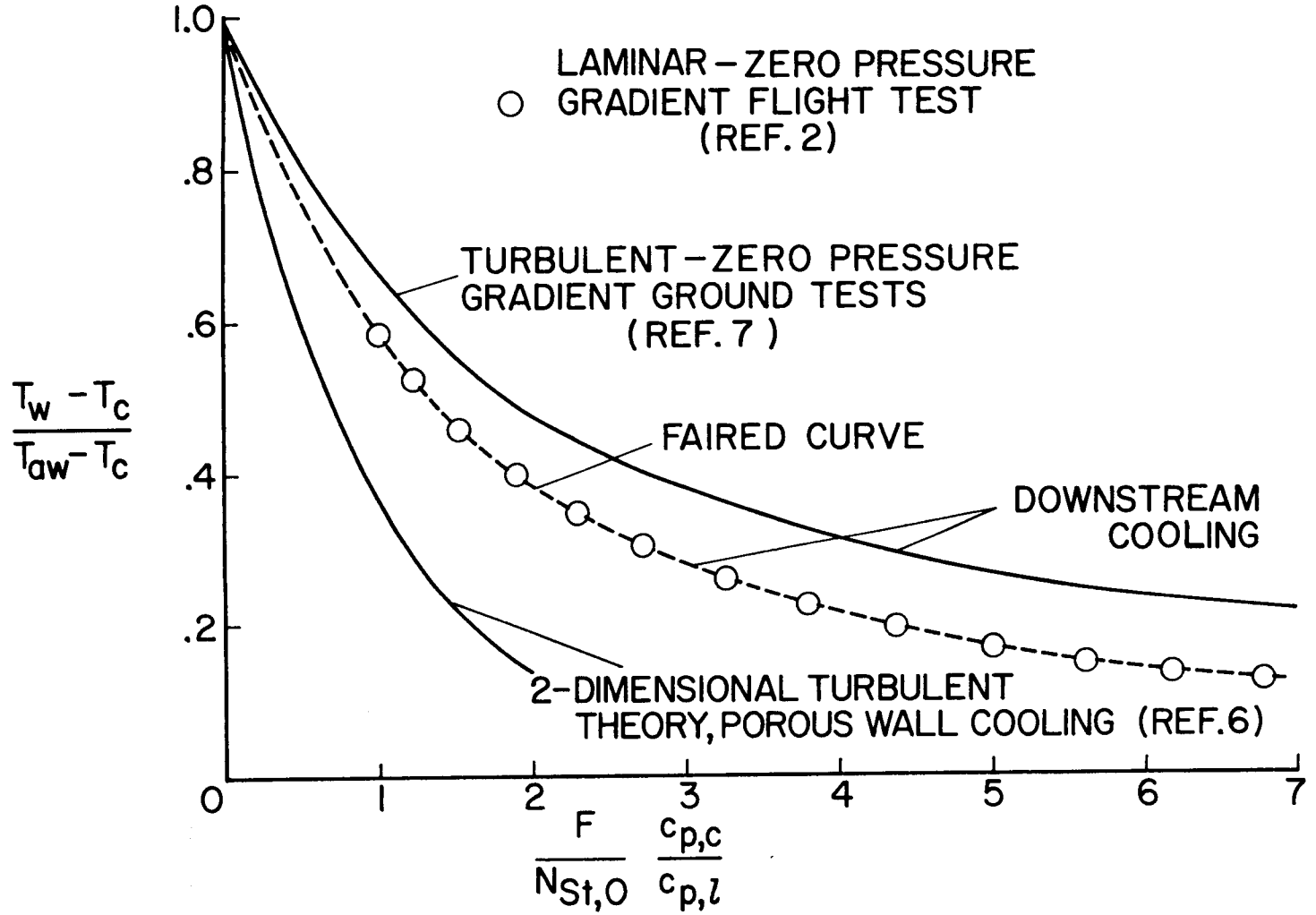

Figure 6.- Downstream cooling test results compared with porous wall cooling.

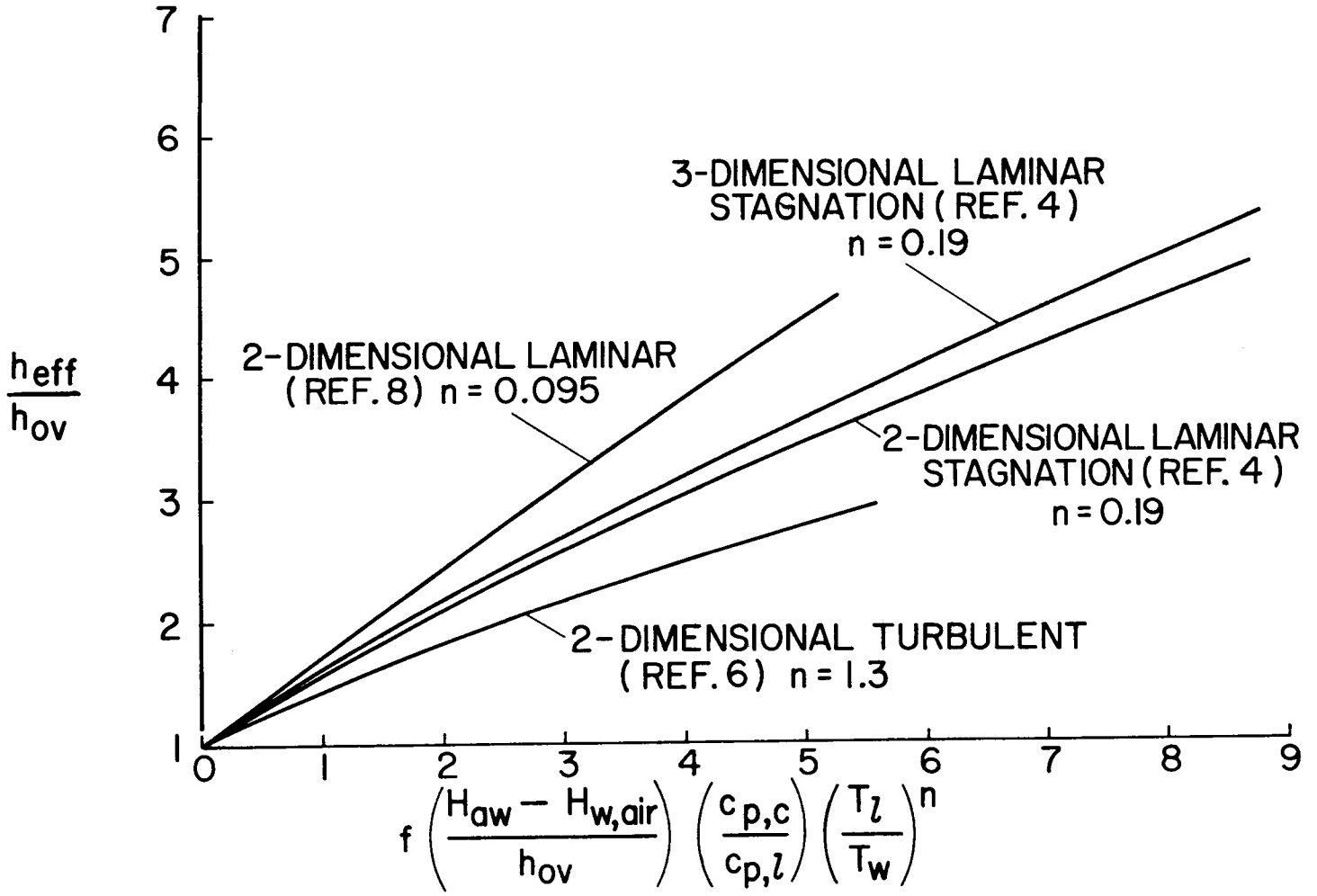

Figure 7.- Effective heats of ablation as a function of enthalpy parameter for several boundary-layer types (ref. 5).

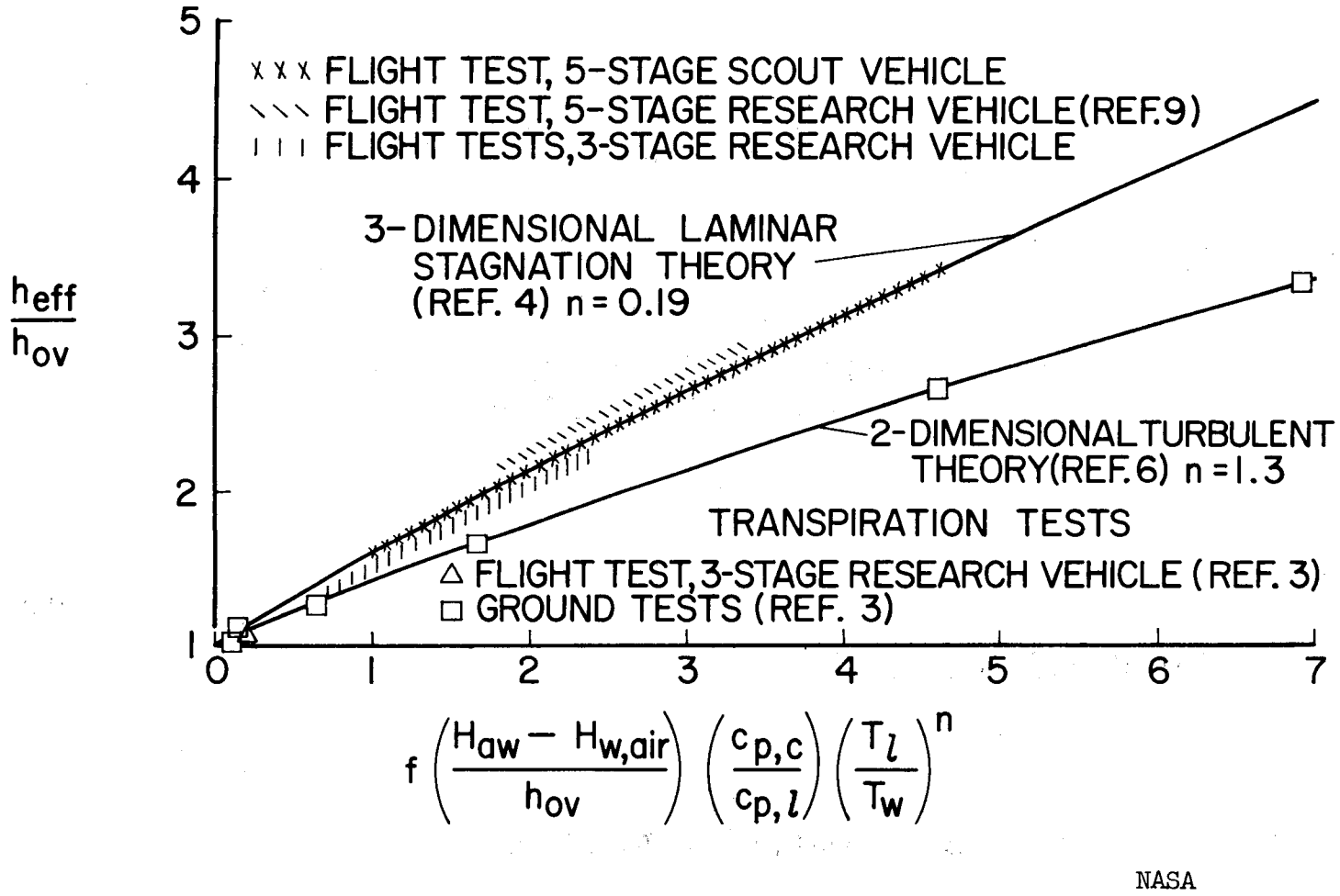

Figure 8.- Effective heat of ablation as a function of enthalpy potential.

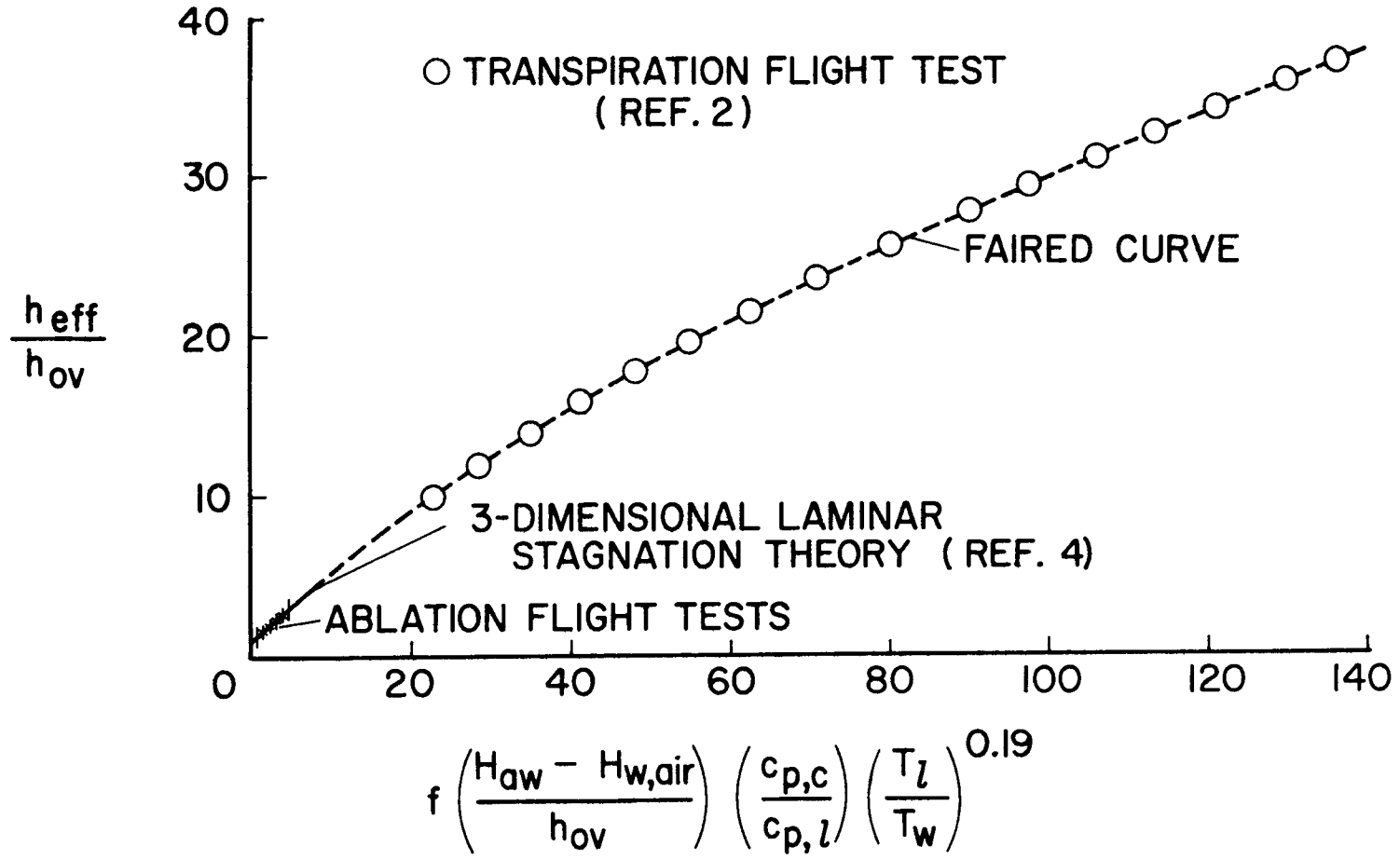

NASA

Figure 9.- Effective heat of ablation as a function of enthalpy potential for a three-dimensional laminar stagnation boundary layer.